J|A|C|S
ARTICLES
Published on Web 05/11/2006

Effect of Side-Chain Substituents on Self-Assembly of Perylene Diimide Molecules: Morphology Control

Kaushik Balakrishnan,† Aniket Datar,† Tammene Naddo,† Jialing Huang,‡ Randy Oitker,† Max Yen,‡ Jincai Zhao,§ and Ling Zang*,†

Contribution from the Department of Chemistry and Biochemistry, Southern Illinois University, Carbondale, Illinois 62901, Materials Technology Center (MTC), Southern Illinois University, Carbondale, Illinois 62901, and Key Laboratory of Photochemistry, Institute of Chemistry, Chinese Academy of Sciences, Beijing 100080, China

Received March 28, 2006; E-mail: lzang@chem.siu.edu

Abstract: Effect of side-chain substitutions on the morphology of self-assembly of perylene diimide molecules has been studied with two derivatives modified with distinctly different side-chains, *N*,*N*′-di(dodecyl)-perylene-3,4,9,10-tetracarboxylic diimide (DD-PTCDI) and *N*,*N*′-di(nonyldecyl)-perylene-3,4,9,10-tetracarboxylic diimide (ND-PTCDI). Due to the different side-chain interference, the self-assembly of the two molecules results in totally different morphologies in aggregate: one-dimensional (1D) nanobelt vs zero-dimensional (0D) nanoparticle. The size, shape, and topography of the self-assemblies were extensively characterized by a variety of microscopies including SEM, TEM, AFM, and fluorescence microscopy. The distinct morphologies of self-assembly have been obtained from both the solution-based processing and surface-supported solvent-vapor annealing. The nanobelts of DD-PTCDI fabricated in solution can feasibly be transferred to both polar (e.g., glass) and nonpolar (e.g., carbon) surfaces, implying the high stability of the molecular assembly (due to the strong $\pi-\pi$ stacking). The side-chain-dependent molecular interaction was comparatively investigated using various spectrometries including UV−vis absorption, fluorescence, X-ray diffraction, and differential scanning calorimetry. Compared to the emission of ND-PTCDI aggregate, the emission of DD-PTCDI aggregate was significantly red-shifted (ca. 30 nm) and the emission quantum yield decreased about three times, primarily due to the more favorable molecular stacking for DD-PTCID. Moreover, the aggregate of DD-PTCDI shows a pronounced absorption band at the longer wavelength, whereas the absorption of ND-PTCDI aggregate is not significant in the same wavelength region. These optical spectral observations are reminiscent of the previous theoretical investigation on the side-chain-modulated electronic properties of PTCDI assembly.

Introduction

Molecules of perylene tetracarboxylic diimide (PTCDI) form a unique class of n-type semiconductor,[1−4] in comparison to the more common p-type counterpart in organic semiconductors. Bulk-phase materials of PTCDI have been widely used in various optoelectronics devices.[1,5,6] Typical examples include thin-film transistors,[4,7,8] photovoltaics,[9−14] liquid crystals,[15,16] and light-emitting diodes.[17−20] Due to their high thermal and photostability, PTCDI molecules have also attracted increasing interest in fabrication of single-molecule devices such as fluorescence switches,[21,22] sensors,[23−26] molecular wires, and transistors.[2,3] However, the self-assembled nanostructures (i.e.,

† Department of Chemistry and Biochemistry, Southern Illinois University.
‡ MTC, Southern Illinois University.
§ Institute of Chemistry, Chinese Academy of Sciences.

(1) Newman, C. R.; Frisbie, C. D.; da Silva Filho, D. A.; Bredas, J.-L.; Ewbank, P. C.; Mann, K. R. *Chem. Mater.* **2004**, *16*, 4436−4451.
(2) Xu, B. Q.; Xiao, X.; Yang, X.; Zang, L.; Tao, N. J. *J. Am. Chem. Soc.* **2005**, *127*, 2386-2387.
(3) Li, X.; Xu, B. Q.; Xiao, X.; Yang, X.; Zang, L.; Tao, N. J. *Faraday Discuss.* **2006**, *131*, 111−120.
(4) Horowitz, G.; Kouki, F.; Spearman, P.; Fichou, D.; Nogues, C.; Pan, X.; Garnier, F. *Adv. Mater.* **1996**, *8*, 242−245.
(5) Wurthner, F. *Chem. Commun.* **2004**, 1564−1579.
(6) Law, K.-Y. *Chem. Rev.* **1993**, *93*, 449−486.
(7) Chesterfield, R. J.; McKeen, J. C.; Newman, C. R.; Ewbank, P. C.; Da Silva Filho, D. A.; Bredas, J.-L.; Miller, L. L.; Mann, K. R.; Frisbie, C. D. *J. Phys. Chem. B* **2004**, *108*, 19281−19292.
(8) Jones, B. A.; Ahrens, M. J.; Yoon, M.-H.; Facchetti, A.; Marks, T. J.; Wasielewski, M. R. *Angew. Chem., Int. Ed.* **2004**, *43*, 6363−6366.
(9) Schmidt-Mende, L.; Fechtenkotter, A.; Mullen, K.; Moons, E.; Friend, R. H.; MacKenzie, J. D. *Science* **2001**, *293*, 1119−1122.
(10) Gregg, B. A. *J. Phys. Chem. B* **2003**, *107*, 4688−4698.
(11) Gregg, B. A. *J. Phys. Chem.* **1996**, *100*, 852−859.
(12) Tamizhmani, G.; Dodelet, J. P.; Cote, R.; Gravel, D. *Chem. Mater.* **1991**, *3*, 1046−1053.
(13) Liu, Y.; Xiao, S.; Li, H.; Li, Y.; Liu, H.; Lu, F.; Zhuang, J.; Zhu, D. *J. Phys. Chem. B* **2004**, *108*, 6256−6260.
(14) Peeters, E.; Van Hal, P. A.; Meskers, S. C. J.; Janssen, R. A. J.; Meijer, E. W. *Chem. Eur. J.* **2002**, *8*, 4470−4474.
(15) Struijk, C. W.; Sieval, A. B.; Dakhorst, J. E. J.; van Dijk, M.; Kimkes, P.; Koehorst, R. B. M.; Donker, H.; Schaafsma, T. J.; Picken, S. J.; van de Craats, A. M.; Warman, J. M.; Zuihof, H.; Sudholter, E. J. R. *J. Am. Chem. Soc.* **2000**, *122*, 11057−11066.
(16) Rohr, U.; Schilichting, P.; Bohm, A.; Gross, M.; Meerholz, K.; Brauchle, C.; Mullen, K. *Angew. Chem., Int. Ed.* **1998**, *37*, 1434−1437.
(17) Alibert-Fouet, S.; Dardel, S.; Bock, H.; Oukachmih, M.; Archambeau, S.; Seguy, I.; Jolinat, P.; Destruel, P. *Chem. Phys. Chem.* **2003**, *4*, 983−985.
(18) Schouwink, P.; Schafer, A. H.; Seidel, C.; Fuchs, H. *Thin Solid Films* **2000**, *372*, 163−168.
(19) Ranke, P.; Bleyl, I.; Simmerer, J.; Haarer, D.; Bacher, A.; Schmidt, H. W. *Appl. Phys. Lett.* **1997**, *71*, 1332−1334.
(20) Zukawa, T.; Naka, S.; Okada, H.; Onnagawa, H. *J. Appl. Phys.* **2002**, *91*, 1171−1174.
(21) Zang, L.; Liu, R.; Holman, M. W.; Nguyen, K. T.; Adams, D. M. *J. Am. Chem. Soc.* **2002**, *124*, 10640−10641.

 10.1021/ja061810z CCC: $33.50

the intermediate state between molecules and bulk materials) of PTCDI molecules have not yet been extensively studied. Although some organized structures (e.g., particles, networks) have been fabricated,[27−32] the one-dimensional (1D) self-assembly (e.g., nanowire) of PTCDI molecules remains challenging.[33]

Well-defined nanowires are ideal building blocks for nanoscale optoelectronic devices for which the device miniaturization requires small channel materials. Whereas nanowires have feasibly been fabricated from conducting polymers such as polyaniline,[34−38] polyacetylene,[39,40] polypyrrole,[41−43] and poly(phenylene vinylene),[44,45] the molecular packing of polymer assembly is often difficult to control due to the complicated intermolecular interactions and polydispersity of the chain. Recent evidence suggests that $\pi-\pi$ interaction can be modulated to facilitate the molecular stacking in self-assembly of conjugated oligomers[46] and planar aromatic molecules.[5,47−49] This is particularly evident in the larger discotic molecules such as hexabenzocoronene.[26,50,51] However, most of these materials are p-type semiconductors. Since electronic devices require both p- and n-type materials, fabrication and characterization of 1D nanostructures with n-type semiconductors (like PTCDI) would provide more insight and guidance into the development of organic-material-based devices.

The main challenge of 1D self-assembly of PTCDI molecules lies in controlling and optimizing the strong $\pi-\pi$ interaction between the perylene planes in cooperation with the hydrophobic interactions between the side chains linked at the two imide positions. In other words, self-assembling PTCDI molecules into 1D structure represents a balance between molecular stacking and solubility. On one hand, a sufficient solubility is crucial for the solution processing of individual molecules, and this requires appropriate side-chain modification (e.g., substitution with long and/or branched alkyl groups) to hinder the $\pi-\pi$ stacking of perylene backbones,[52] but on the other hand, such a weakened $\pi-\pi$ stacking prevents the effective packing of PTCDI molecules along one dimension. One way to enhance the molecular packing is to increase the size of the core aromatic system, i.e., to change the PTCDI monomer to a trimer, tetramer, or pentamer.[5,31,53] In some cases, the enlarged PTCDI molecules favor the formation of fibril structures, whereas the molecular packing is not highly optimized. The twisting between the PTCDI units (due to energy minimization) in the supramolecules weakens the $\pi-\pi$ interaction between molecules and thus distorts the molecular packing from the co-facial conformation, leading to a molecular assembly deviated from 1D morphology.

As previously observed by theoretical calculation and experimental characterization (particularly X-ray diffraction), the side chain of PTCDI plays a crucial role in controlling the molecular packing conformation (and thus the electronic structure of the assembly).[5,54,55] For example, changing the side chain from ethoxyethyl to methoxypropyl (*two structurally similar moieties!*) transforms the color of the PTCDI aggregate from red to black (the absorption maximum changes from 564 to 613 nm and the band broadens considerably).[54] Obviously, the observed spectral change in these solids is the manifestation of an aggregation effect because both of the two molecules have essentially the same absorption spectra in solution. Such a sensitive side-chain modulation provides a potentially effective way to control and optimize the molecular packing conformation, enabling the 1D growth of the self-assembly. Moreover, the two nitrogen positions at the imides of PTCDI are nodes in the π-orbital wave function,[52,55] providing enormous options for modifying the structures of the two side chains (but without significant alteration of the electronic property of the PTCDI molecule). This makes it feasible to examine the side-chain effect on the molecular packing conformation and hence the morphology of the molecular self-assembly.

The other factor affecting the morphology of molecular self-assembly is the solvent−molecule interaction, which counterbalances the intermolecular interactions (particularly the hydrophobic interaction between side chains). Selection of solvent is usually a critical step toward successful assembly of well-defined structures (e.g., nanowires). In general, a 'poor' solvent (which

(22) Gronheid, R.; Stefan, A.; Cotlet, M.; Hofkens, J.; Qu, J.; Muellen, K.; Van der Auweraer, M.; Verhoeven, J. W.; De Schryver, F. C. *Angew. Chem., Int. Ed.* **2003**, *42*, 4209−4214.
(23) Liu, R.; Holman, M. W.; Zang, L.; Adams, D. M. *J. Phys. Chem. A* **2003**, *107*, 6522−6526.
(24) Holman, M. W.; Liu, R.; Zang, L.; Yan, P.; DiBenedetto, S. A.; Bowers, R. D.; Adams, D. M. *J. Am. Chem. Soc.* **2004**, *126*, 16126−16133.
(25) Sauer, M. *Angew. Chem., Int. Ed.* **2003**, *42*, 1790−1793.
(26) Grimsdale Andrew, C.; Mullen, K. *Angew. Chem., Int. Ed.* **2005**, *44*, 5592−5629.
(27) Wang, W.; Li, L.-S.; Helms, G.; Zhou, H.-H.; Li, A. D. Q. *J. Am. Chem. Soc.* **2003**, *125*, 1120−1121.
(28) Sugiyasu, K.; Fujita, N.; Shinkai, S. *Angew. Chem., Int. Ed.* **2004**, *43*, 1229−1233.
(29) Van Herrikhuyzen, J.; Syamakumari, A.; Schenning, A. P. H. J.; Meijer, E. W. *J. Am. Chem. Soc.* **2004**, *126*, 10021−10027.
(30) van der Boom, T.; Hayes, R. T.; Zhao, Y.; Bushard, P. J.; Weiss, E. A.; Wasielewski, M. R. *J. Am. Chem. Soc.* **2002**, *124*, 9582−9590.
(31) Ahrens, M. J.; Sinks, L. E.; Rybtchinski, B.; Liu, W.; Jones, B. A.; Giaimo, J. M.; Gusev, A. V.; Goshe, A. J.; Tiede, D. M.; Wasielewski, M. R. *J. Am. Chem. Soc.* **2004**, *126*, 8284−8294.
(32) Schenning, A. P. H. J.; Herrikhuyzen, J. V.; Jonkheijm, P.; Chen, Z.; Wurthner, F.; Meijer, E. W. *J. Am. Chem. Soc.* **2002**, *124*, 10252−10253.
(33) Schenning, A. P. H. J.; Meijer, E. W. *Chem. Commun.* **2005**, 3245−3258.
(34) Huang, J. X.; Virji, S.; Weiller, B. H.; Kaner, R. B. *J. Am. Chem. Soc.* **2003**, *125*, 314−315.
(35) Zhou, Y.; Freitag, M.; Hone, J.; Staii, C.; Johnson, J. A. T. *Appl. Phys. Lett.* **2003**, *83*, 3800−3802.
(36) Liu, H.; Kameoka, J.; Czaplewski, D. A.; Craighead, H. G. *Nano Lett.* **2004**, *4*, 671−675.
(37) Virji, S.; Huang, J.; Kaner, R. B.; Weiller, B. H. *Nano Lett.* **2004**, *4*, 491−496.
(38) Huang, J.; Virji, S.; Weiller, B. H.; Kaner, R. B. *Chem. Eur. J.* **2004**, *10*, 1314−1319.
(39) Lee, H. J.; Jin, Z. X.; Aleshin, A. N.; Lee, J. Y.; Goh, M. J.; Akagi, K.; Kim, Y. S.; Kim, D. W.; Park, Y. W. *J. Am. Chem. Soc.* **2004**, *126*, 16722−16723.
(40) Gan, H.; Liu, H.; Li, Y.; Zhao, Q.; Li, Y.; Wang, S.; Jiu, T.; Wang, N.; He, X.; Yu, D.; Zhu, D. *J. Am. Chem. Soc.* **2005**, *127*, 12452−12453.
(41) Zhang, X.; Manohar, S. K. *J. Am. Chem. Soc.* **2005**, *127*, 14156−14157.
(42) Bocharova, V.; Kiriy, A.; Vinzelberg, H.; Moench, I.; Stamm, M. *Angew. Chem., Int. Ed.* **2005**, *44*, 6391−6394.
(43) Berdichevsky, Y.; Lo, Y.-H. *Adv. Mater. (Weinheim, Ger.)* **2006**, *18*, 122−125.
(44) Luo, Y. H.; Liu, H. W.; Xi, F.; Li, L.; Jin, X. G.; Han, C. C.; Chan, C. M. *J. Am. Chem. Soc.* **2003**, *125*, 6447−6451.
(45) Jeukens, C. R. L. P. N.; Jonkheijm, P.; Wijnen, F. J. P.; Gielen, J. C.; Christianen, P. C. M.; Schenning, A. P. H. J.; Meijer, E. W.; Maan, J. C. *J. Am. Chem. Soc.* **2005**, *127*, 8280−8281.
(46) Hoeben, F. J. M.; Jonkheijm, P.; Meijer, E. W.; Schenning, A. P. H. J. *Chem. Rev.* **2005**, *105*, 1491−1546.
(47) Nguyen, T.-Q.; Martel, R.; Avouris, P.; Bushey, M. L.; Brus, L.; Nuckolls, C. *J. Am. Chem. Soc.* **2004**, *126*, 5234−5242.
(48) Shirakawa, M.; Fujita, N.; Shinkai, S. *J. Am. Chem. Soc.* **2005**, *127*, 4164−4165.
(49) Wang, Z.; Medforth, C. J.; Shelnutt, J. A. *J. Am. Chem. Soc.* **2004**, *126*, 15954−15955.
(50) Kastler, M.; Pisula, W.; Wasserfallen, D.; Pakula, T.; Mullen, K. *J. Am. Chem. Soc.* **2005**, *127*, 4286−4296.
(51) Hill, J. P.; Jin, W.; Kosaka, A.; Fukushima, T.; Ichihara, H.; Shimomura, T.; Ito, K.; Hashizume, T.; Ishii, N.; Aida, T. *Science* **2004**, *304*, 1481−1483.
(52) Langhals, H. *Heterocycles* **1995**, *40*, 477−500.
(53) Yan, P.; Chowdhury, A.; Holman, M. W.; Adams, D. M. *J. Phys. Chem. B* **2005**, *109*, 724−730.
(54) Klebe, G.; Graser, F.; Hadicke, E.; Berndt, J. *Acta Crystallogr.* **1989**, *B45*, 69−77.
(55) Kazmaier, P. M.; Hoffmann, R. *J. Am. Chem. Soc.* **1994**, *116*, 9684−9691.

Chart 1. Molecular Structures of ND- and DD-PTCDI

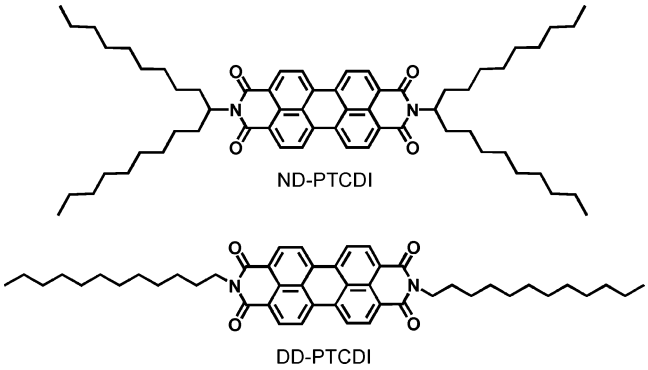

has limited solubility for the molecules due to the weak solvent−molecule interaction) is suited for facilitating the molecular assembly. For some PTCDI molecules with short, linear side chains, 1D assembly can simply be obtained by dispersing a concentrated solution into a 'poor' solvent.[56] However, for the molecules with long alkyl side chains (possessing strong hydrophobic interaction), the aggregation often proceeds too fast (due to the enhanced intermolecular association) for the molecular assembly to grow along one direction, thus leading to formation of chunky aggregates rather than nanowires. To this end, highly controlled solution processing has to be employed to optimize the molecular stacking kinetics. Indeed, solution-based processing plays more with the kinetics of molecular assembling than the thermodynamics of molecules (energy-minimized molecular packing conformation), which is mainly determined by the molecular structure. Prior to judging if a molecule is thermodynamically suited or not for 1D assembly, one must ensure that the assembling has been processed under the optimized conditions or at least been examined through various comparative processes. This is critical for studying the side-chain effect on the molecular self-assembly. Otherwise, it would be risky to assign a failure of 1D fabrication simply to the 'inappropriate' molecular structure (i.e., the thermodynamic reason).

Beyond the solution processing methods, a solvent-vapor annealing technique has successfully been used for self-assembling 1D nanostructures of PTCDI molecules on substrates.[57] Such an approach provides in situ preparation of nanowires on a surface (e.g., glass) that is suited for optical or microscopy investigation. More importantly, the solvent-vapor annealing enables slow crystallization (molecular assembling), which allows molecules to find the most stable packing conformation, providing an alternative way to examine the side-chain effect on the dimensionality of self-assembly.

Herein, we report on an extensive, comparative investigation of the self-assembly of two PTCDI molecules with different side chains, dodecyl (DD) vs nonyldecyl (ND) (Chart 1). These two side chains are similar in length but dramatically different in configuration, thus demanding different conformations of molecular stacking. DD-PTCDI molecules are expected to favor 1D molecular assembly due to the hydrophobic interaction between the linear side-chains being highly cooperative with the $\pi-\pi$ interaction between perylene planes, while for ND-PTCDI molecules, the steric hindrance of side chains interferes with molecular packing, preventing the self-assembly to grow along one dimension. Indeed, as shown in this study, 1D nanostructures (i.e., nanobelts) have been fabricated from DD-PTCDI, whereas 0D nanospheres have been obtained for ND-PTCDI. Strikingly, such a difference in morphology was observed for both the solution-based processing and surface-assisted solvent-vapor annealing, which were employed to approach comparative self-assembling of the two molecules. The investigation presented demonstrates the potential control over the dimensionality of self-assembly of PTCDI molecules through appropriate molecular design (particularly the side-chain modification) in line with proper assembly processing that matches the best the thermodynamics of the molecular structure.

Results and Discussion

1. Spectral Characterization in Solutions. The absorption spectrum of PTCDI normally shows three pronounced peaks (in the range of 450−525 nm) and a shoulder around 425 nm, which correspond to the 0−0, 0−1, 0−2, and 0−3 electronic transitions, respectively. The fluorescence spectrum depicts the same peak structure in a mirror image of the absorption. Since the two nitrogen positions at the imides are node in π orbitals,[52,55] substitution of the side chain with different moieties does not change the electronic structure of the PTCDI molecule, making it feasible to use optical spectrometry to characterize the molecular assembly of the PTCDI molecules with different side chains.

When dispersed in 'poor' solvents (e.g., methanol, acetonitrile, DMSO, and hexane), DD-PTCDI molecules undergo aggregation due to the limited solubility, as depicted by the dramatic change in the absorption spectra (Figure 1A). A new band emerges around 565 nm, and the transitions from ground state to the higher levels of electronic states (0−1, 0−2, and 0−3) are enhanced compared to the 0−0 transition. Such a spectral change implies strong molecular stacking between the PTCDI skeletons.[5] The pronounced absorption band emerging at longer wavelength is typically a sign of the effective $\pi-\pi$ interaction in co-facial configuration of molecular stacking.[5,55,56,58] As a result, the fluorescence of the molecule was significantly quenched due to the $\pi-\pi$ electronic coupling (Figure 1B), which splits the π orbitals of PTCDI into two bands with the higher-energy band possessing most of the oscillator strength.[5,31] From the decreased emission, one can estimate the percentage of molecules transformed into aggregate by comparing the emission intensity with that of DD-PTCDI molecules in a homogeneous solution (Figure S1A and B). The quantum yield of fluorescence of PTCDI molecules in 'good' solvents (i.e., homogeneous solutions) is usually close to unity.[52]

For a diluted suspension of molecular aggregate of DD-PTCDI, excitation at the absorption band ($\sim$ 565 nm) of the crystalline phase did not produce detectable emission, mainly due to the symmetry-forbidden transition involving the lower-energy π-stacking state.[5,31,56] To detect the weak emission of such aggregate, the measurement should be based on a sufficient amount of materials, for example, a solid sample cast on glass (as discussed below).

In contrast, ND-PTCDI is soluble in almost all the organic solvents due to the branched structure of the side chain. To

(56) Balakrishnan, K.; Datar, A.; Oitker, R.; Chen, H.; Zuo, J.; Zang, L. *J. Am. Chem. Soc.* **2005**, *127*, 10496−10497.
(57) Datar, A.; Oitker, R.; Zang, L. *Chem. Commun.* **2006**, 1649−1651.
(58) Hadicke, E. H.; Graser, F. *Acta Crystallogr.* **1986**, *C42*, 189−195.

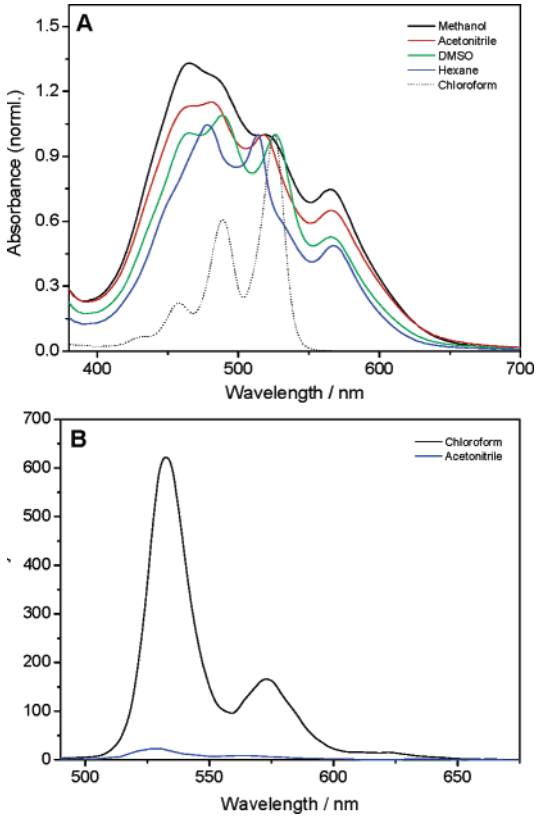

Figure 1. UV−vis absorption (A) and fluorescence (B) spectra of DD-PTCDI (5 μM) in 'poor' solvents. For comparison, the absorption spectrum of a homogeneous solution in chloroform is also depicted. The absorption spectra are normalized at the 0−0 transition maximum.

facilitate the aggregation of molecules, one has to use a mixed solvent composed of an organic solvent and water (in which the molecule is not soluble at all). As shown in Figure 2A, upon dispersion into a binary solvent of 35:65 water/methanol, ND-PTCDI molecules assemble into the solid state, resulting in dramatic change in absorption spectrum. The relatively higher absorption at shorter wavelength implies the enhanced transition of 0−1 and 0−2 due to the $\pi-\pi$ interaction within the molecular aggregate. However, there was no pronounced absorption band emerging at the longer wavelength, except for a long tail of absorption extending into the red. Compared to the absorption of individual molecules of ND-PTCDI, the absorption of the assembly was red-shifted, generally consistent with the enhanced molecular interaction in aggregate. The lack of formation of new, pronounced absorption band at longer wavelength implies the weak (distorted) $\pi-\pi$ interaction in the aggregate of ND-PTCDI compared to that of DD-PTCDI.

More interestingly, there was no emission of individual molecules detected from the suspension of ND-PTCDI in the binary solvent of 35:65 water/methanol (Figure 2B), implying that all the molecules were assembled into aggregate due to the poor solubility in such a solvent. However, a significant, red-shifted emission ($\lambda_{max} \approx 604$ nm, quantum yield $\approx 7\%$) was measured for the aggregate phase. With excitation at different wavelengths (ranging from 400 to 550 nm), the emission band demonstrated the same shape and centered at the same wavelength, indicating that the emission is originated from the lowest excimer-like excited state.[5,31] Such an excimer-like state is usually weakly emitting (due to the symmetry-forbidden transition to the ground state) for the molecular

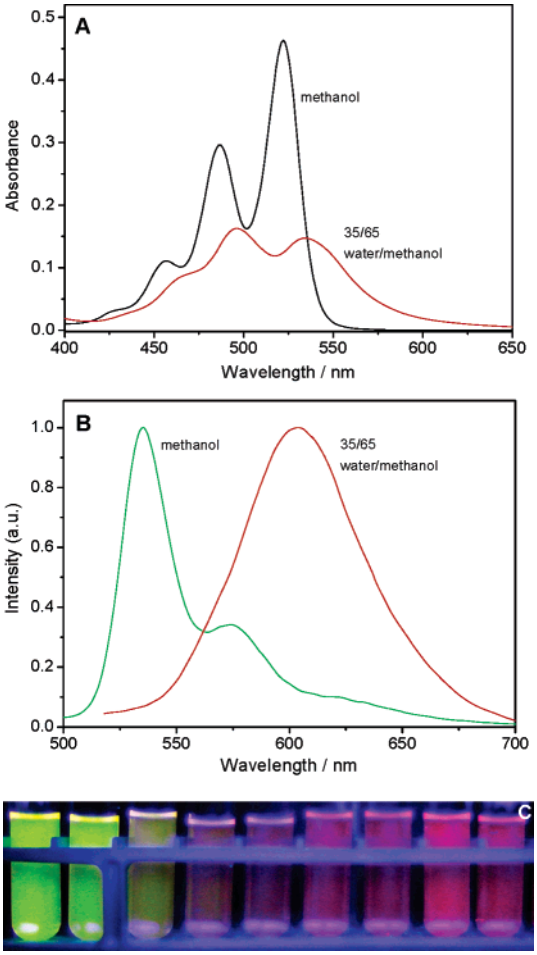

Figure 2. UV−vis absorption (A) and fluorescence (B) spectra of ND-PTCDI (6 μM) in pure methanol and 35:65 water/methanol binary solvents. The fluorescence spectra are normalized to reveal the band shift. Excitation at different wavelengths produced the fluorescence spectra in the same shape and centered at the same wavelength. (C) The color of fluorescence emission of ND-PTCDI (5 μM) is tuned in a series of water/methanol binary solvents containing (from left to right) 0%, 1%, 3%, 7%, 12%, 17%, 23%, 30%, and 35% water.

aggregate with strong $\pi-\pi$ stacking, as observed for PTCDI molecules with linear side chains.[56] The relatively high fluorescence observed for the ND-PTCDI assembly is likely due to the distorted molecular packing (caused by the branched side chains). Continuously changing the volume ratio of water/methanol from 0:100 to 35:65 led to a gradual transformation of free molecules of ND-PTCDI into the aggregate. As shown in Figure 2C, the emission color detected from the suspension was gradually tuned from bright green (for the totally free dispersed molecules) to bright red (for the molecular aggregate).

Since the electronic properties of DD- and ND-PTCDI are essentially the same when dispersed as free molecules (see Figures S1 and S2), the strikingly different absorption and fluorescence spectra observed for the aggregate states of the two molecules are most likely due to the different molecular packing conformation, which in turn determines the optical spectral property of the molecular assembly.[54,55] As seen below, such a different molecular packing conformation results in a different dimensional preference for the growth of the molecular assembly.

Solubility of molecules is dependent on temperature. For the DD-PTCDI molecules dispersed in a 'poor' solvent, the solubil-

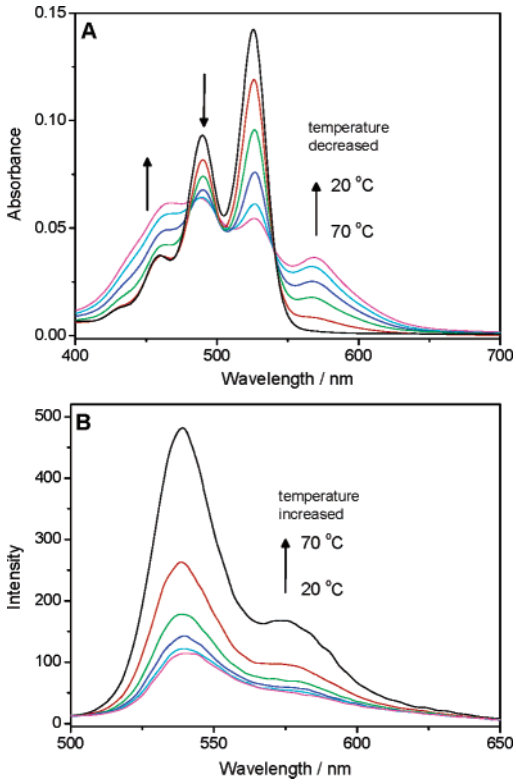

Figure 3. UV−vis absorption (A) and fluorescence (B) spectra of DD-PTCDI (5 μM) in DMSO at different temperatures.

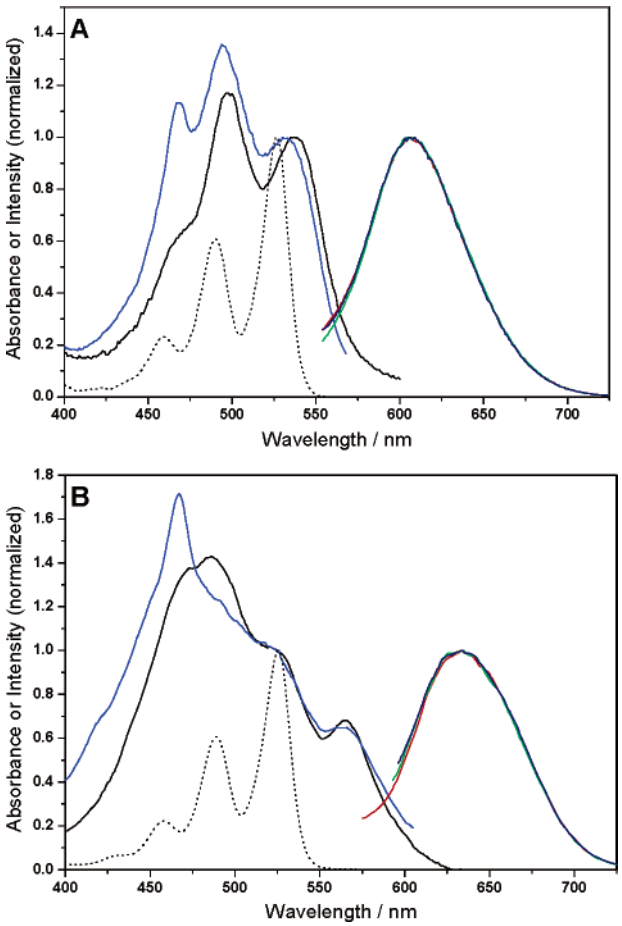

Figure 4. UV−vis absorption (black) and fluorescence excitation (blue) and emission spectra of a thin film of ND-PTCDI (A) and DD-PTCDI (B) spin-cast on glass from a chloroform solution (0.5 mM for ND-PTCDI, 0.38 mM for DD-PTCDI). Emission spectra were recorded at three excitation wavelengths: 468 (red), 497 (green), and 530 nm (navy) for ND-PTCDI; 465 (red), 490 (green), and 520 nm (navy) for DD-PTCDI. The excitation spectrum was recorded at the maximum emission wavelength of 607 nm for ND-PTCDI and 635 nm for DD-PTCDI. The absorption spectrum of homogeneous chloroform solution (dotted line) is also shown for comparison.

ity could be increased by heating the solution. As shown in Figure 3A, a 5 μM solution of DD-PTCDI in DMSO at room temperature demonstrated an absorption spectrum typical of a molecular aggregate, for which a new, prominent absorption band emerged at the longer wavelength compared to the absorption of individual molecules. Heating the suspension up to 70 °C caused a gradual change in absorption spectra, with disappearance of the long-wavelength band and decrease in the absorption at shorter wavelengths (the transitions of 0−1, 0−2, and 0−3). An isobestic point at 540 nm indicates the stoichiometric transformation between the aggregate and free molecules. Above 70 °C, most of the DD-PTCDI molecules are freely dispersed in the solvent. Consistent with the absorption measurement, the molecular fluorescence of the DMSO solution was increased with an increase in the temperature (Figure 3B), indicating more free molecules were dissociated from the aggregate upon heating. Similar temperature-induced spectral change was also observed for DD-PTCDI in other 'poor' solvents (e.g., 2-propanol, methyl cyclohexane, and heptane) as shown in Figure S3. These observations imply that the self-assembling of DD-PTCDI can feasibly be processed in various 'poor' solvents at room temperature, at which the molecular association is thermodynamically favorable.

2. Characterizing Molecular Packing in the Solid State. Figure 4A shows the absorption spectrum of a thin film of ND-PTCDI spin-cast on glass from a concentrated solution in chloroform (0.5 mM). The band structure of the absorption resembles that of the nanocrystals suspended in solution (shown in Figure 2A), implying the same molecular packing conformation in the two cases. Compared to the absorption of free molecules in chloroform (also shown in Figure 4A), the 0−1 and 0−2 transitions became dramatically enhanced upon aggregation of molecules. The film of ND-PTCDI demonstrated significant fluorescence centered at 607 nm. Changing the excitation wavelength in the range of 450−550 nm did not change the position or shape of the emission spectra, indicating that the emission originates from the lowest excimer state (formed by the molecular stacking). Such an observation is consistent with that observed in solutions (Figure 2B). Figure 4A also shows the fluorescence excitation spectrum of the film of ND-PTCDI. Interestingly, compared to the absorption spectrum, the excitation spectrum shows higher transition efficiency at the shorter wavelength (particularly the 0−2 transition). Such a discrepancy was previously observed for the aggregate of other PTCDIs.[11] The decreased emission at excitation of longer wavelength is (although not yet clear) likely due to the symmetry-forbidden transition between the ground state and the lowest-energy excited state, which is not favorable for the excimer-like emission.[5]

The spectra of DD-PTCDI film (Figure 4B) showed significantly different character compared to that of ND-PTCDI (Figure 4A), although the two molecules demonstrate the same absorption (dotted lines in Figure 4A and B) and fluorescence

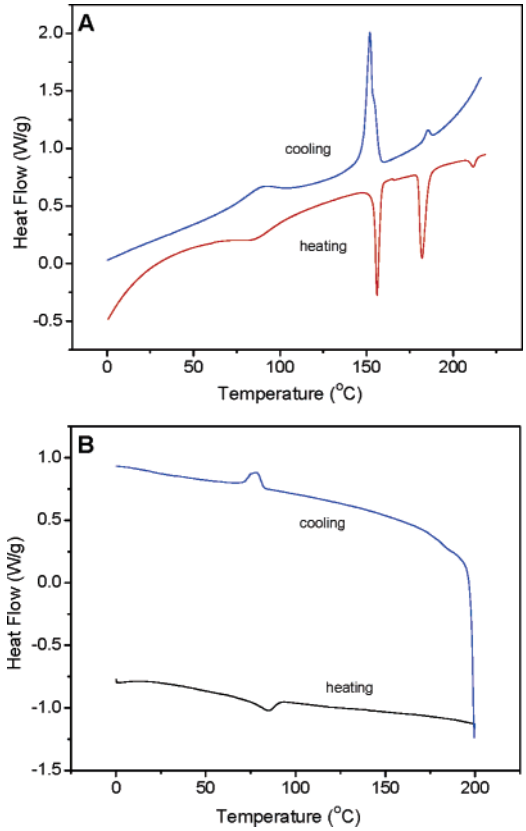

Figure 5. Differential scanning calorimetry (DSC) traces of the solid state of DD-PTCDI (A) and ND-PTCDI (B). The data shown are from the second heating−cooling cycle.

spectra (Figures S1B and S2B) in homogeneous solutions. The emission from DD-PTCDI film centers at 635 nm, about 30 nm red-shifted compared to the emission of ND-PTCDI film. Such a large spectral shift is mainly due to the more favorable $\pi-\pi$ stacking (i.e., stronger molecular interaction) in the molecular assembly of DD-PTCDI.[55] Strong $\pi-\pi$ stacking normally leads to weak emitting crystal phase due to the forbidden low-energy excitonic transition.[5] Indeed, the emission quantum yield of the DD-PTCDI film was about three times lower than that of the ND-PTCDI film. Also consistent with the strong $\pi-\pi$ stacking, the 0−2 transition becomes more predominant over the lower-energy transition (e.g., 0−0 transition), as revealed in the absorption spectrum, and more clearly in the excitation spectrum.

The different extent of $\pi-\pi$ stacking for ND- and DD-PTCDI molecules was also evidenced by the measurement of differential scanning calorimetry (DSC), as shown in Figure 5. The DSC pattern of DD-PTCDI is typical of a liquid crystal material, showing a phase transition between a series of temperatures, whereas ND-PTCDI shows only one phase transition at 85 °C, which corresponds to the melting point. Indeed, the fluid phase of ND-PTCDI can simply be obtained by heating it up in a regular oven above 85 °C. As demonstrated in Figure 5A, the melting point of DD-PTCDI should be far above 200 °C, which is much higher than that of ND-PTCDI. The dramatically lower melting point of ND-PTCDI indicates the weakened (distorted) molecular stacking, which is caused by the strong steric hindrance of the branched side chains. Such a weakened molecular stacking also makes the low-energy excitonic transition allowable,[5] leading to stronger emission of ND-PTCDI

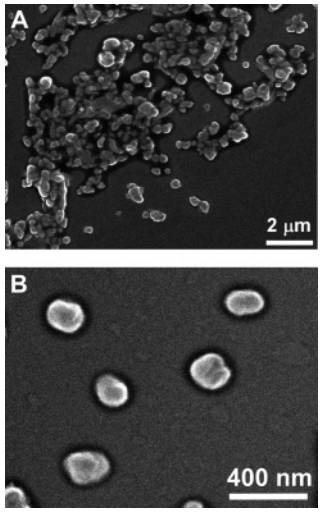

Figure 6. (A) Large-area SEM image of ND-PTCDI aggregates, which were synthesized by dispersing a minimum volume of concentrated chloroform solution (0.5 mM) into a large excess of 35:65 water/methanol, so that the final concentration was 15 μM. The SEM sample was prepared by spin-coating the aggregate suspension on glass at 2000 rpm. (B) A higher-magnification image showing discrete particles in approximately spherical shape.

aggregate compared to that of DD-PTCDI aggregate (as discussed above).

3. Morphology Characterization of Self-Assembly from Solutions. Due to the high solubility in most organic solvents, the self-assembly of ND-PTCDI was performed in a binary solvent of water/methanol (35:65), which enables effective molecular aggregation, as evidenced by the optical spectral measurement (Figure 2). SEM imaging of the molecular assembly spin-cast on glass showed particulate aggregate in an approximately spherical shape, with average size of ~200 nm (Figure 6). The spherical morphology of molecular aggregate is consistent with the distorted $\pi-\pi$ stacking, which prevents the molecules from assembling along one dimension.

In contrast, the favorable $\pi-\pi$ stacking of DD-PTCDI leads to formation of 1D molecular assembly, particularly nanobelt, which was fabricated by phase-transfer self-assembly between excess of hexane and a concentrated chloroform solution (Figure 7). The nanobelts thus obtained show quite uniform morphology in terms of both width and thickness. The average width (as shown in Figure 7B) is ca. 200 nm, and the length is in the range of a few tens of micrometers, leading to an aspect ratio (length over width) in a magnitude of 100. In some areas, some nanobelts show twisted conformation with the edge lifted up, perpendicular to the substrate (Figure 7B), clearly revealing the belt morphology of the assembly. The belt morphology was also revealed by the AFM measurement, as shown in Figure 8. The line-scan profile over a single fiber demonstrates a flat topography typical of a nanobelt. The thickness as measured is ca. 100 nm, leading to an aspect ratio of the belt cross-section (width/thickness) to be around 2:1. Such an aspect ratio is consistent with the unit-cell parameters obtained for the crystals of PTCDI molecules with linear side chains,[58] for which the ratio of the longitudinal and transverse edge-to-edge distances between two adjacent PTCDI molecules is close to 2:1.

The X-ray diffraction measurement of the nanobelts of DD-PTCDI shows the long axis of the unit cell as 24.0 Å (Figure 9), which is about 26% shorter than the total length of a DD-

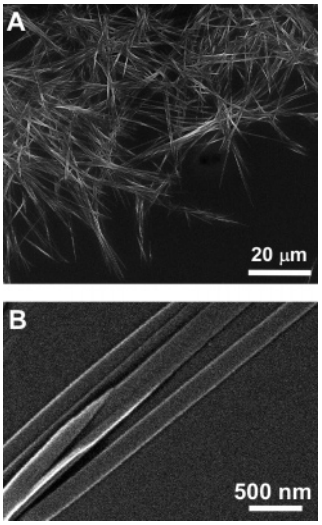

Figure 7. (A) Large-area SEM image of DD-PTCDI nanobelts, which were synthesized by the phase-transfer crystallization between excessive hexane and a concentrated chloroform solution (0.28 mM). The SEM sample was prepared by drop-casting the nanobelt suspension in hexane onto a glass cover slip. More large-area images of the nanobelts are depicted in Figure S5 in the Supporting Information. (B) A higher-magnification image showing discrete, straight nanobelts, on which another belt is piled in a twisted conformation with one edge faced up.

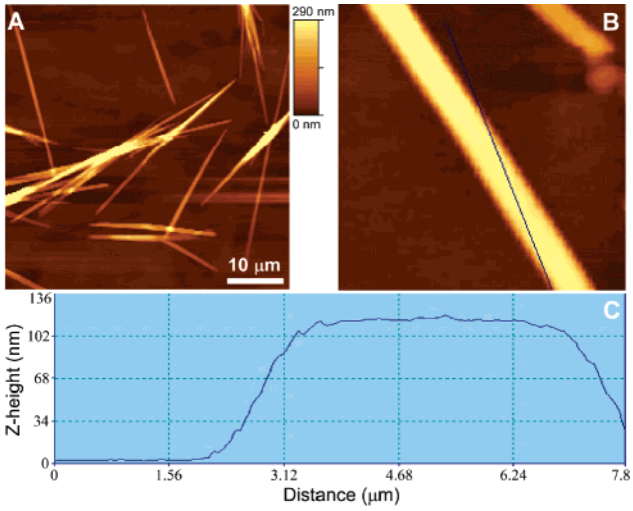

Figure 8. (A) AFM image of DD-PTCDI nanobelts (the same sample shown in Figure 7); (B) A higher-magnification image over a single nanobelt; (C) A line-scan profile (marked in B) clearly reveals the flat top of the nanobelt. The AFM sample was prepared by drop-casting the nanobelt suspension in hexane onto a glass cover slip. One more large-area image of the nanobelts is depicted in the Supporting Information (Figure S9).

PTCDI molecule (along the long axis of PTCDI), 32.6 Å, which was obtained from the energy-optimized conformation of the molecule (DFT calculation, B3LYP/6-311g**//6-31g*). This is likely due to the tilted stacking of PTCDI planes, in line with the strong hydrophobic interaction between side-chains, which usually results in effective side-chain interdigitation and thus leads to shortened length along the longitudinal direction.[54] Significant side-chain interdigitation has previously been observed for other PTCDI molecules with linear side chains.[58,59] In contrast, the nanocrystal of ND-PTCDI shows a shorter long-axis of 19.7 Å (which is beyond the spatial range allowable for

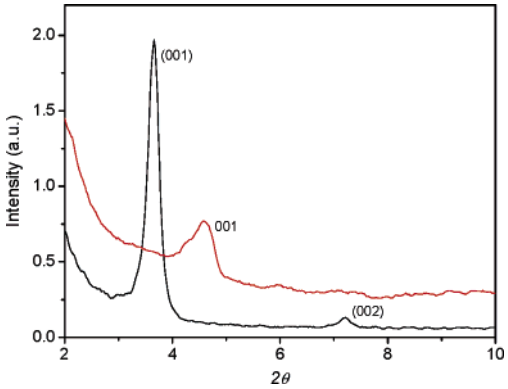

Figure 9. X-ray diffraction pattern of the ND-PTCDI nanocrystals (red) and DD-PTCDI nanobelts (black), the same materials as those used in Figures 6 and 7. The samples were deposited on glass cover slips suited for the X-ray measurement.

side-chain interdigitation), implying a molecular packing distorted from the parallel co-facial conformation.

The nanobelts of DD-PTCDI were also fabricated from the phase transfer between chloroform and other 'poor' solvents such as methanol. Figure 10A and B shows TEM images of the nanobelts deposited on silicon oxide film. Quite uniform nanobelts with large aspect ratio (length over width) were obtained. Some belts in a twisted conformation are clearly revealed by the TEM imaging. As depicted in a zoom-in image (Figure 10B), the average width of the nanobelts is below 100 nm, which is smaller than that obtained from the hexane/chloroform fabrication (as described in Figure 7). Such a difference in size is likely due to the different polarity of hexane and methanol. Although both solvents provide limited solubility for DD-PTCDI and thus facilitate the molecular aggregation, the stronger solvent−molecule interaction between hexane and the dodecyl group may enhance the interdigitation between the side chains of DD-PTCDI, leading to widened nanobelt assembly, as shown in Figure 7.

The same nanobelts of DD-PTCDI were also successfully deposited on holey carbon film and imaged by TEM. As shown in Figure 10C and D, the nanobelts are well dispersed on the carbon film. For the nanobelts lying across a hole, the TEM image shows better contrast due to the ease of focus and astigmatism correction. The overall morphology observed was quite the same as that observed on the silicon oxide substrate (Figure 10A and B), indicating that the preformed molecular packing conformation (morphology) was robust for casting on the substrates with dramatically different polarities. This is reminiscent of the strong molecular stacking as inferred from the spectral measurement described above. High durability of molecular self-assembly (for being transferred from solution onto solid substrate) is critical for approaching practical application of the nano-assembly in electronics. For some nanowires that are formed by weak molecular interactions, the stacks may collapse when casting onto a substrate, with which the component molecule has stronger interaction than the intermolecular interaction.[33,60]

4. Self-Assembly Facilitated by Solvent-Vapor Annealing. The side-chain effect on the molecular stacking conformation

(59) Datar, A.; Balakrishnan, K.; Yang, X. M.; Zuo, X.; Huang, J. L.; Yen, M.; Zhao, J.; Tiede, D. M.; Zang, L. *J. Phys. Chem.* **2006**, submitted.

(60) Jonkheijm, P.; Hoeben, F. J. M.; Kleppinger, R.; Van Herrikhuyzen, J.; Schenning, A. P. H. J.; Meijer, E. W. *J. Am. Chem. Soc.* **2003**, *125*, 15941−15949.

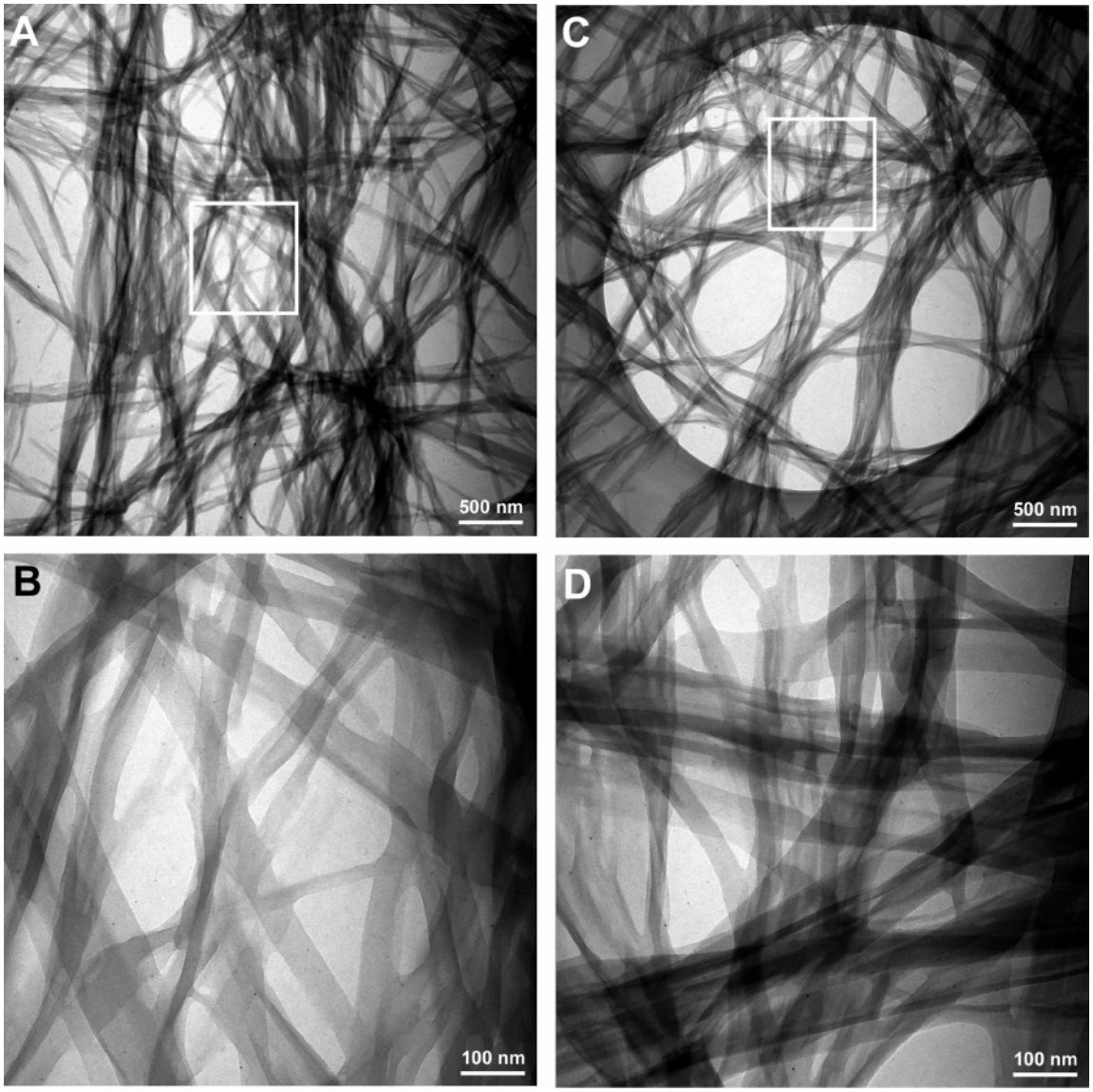

Figure 10. Large-area TEM images of DD-PTCDI nanobelts deposited on silicon oxide film (A) and holey carbon film (C). B and D show the zoomed-in images of A and C, respectively. The nanobelts were synthesized by the phase-transfer crystallization between excessive methanol and a concentrated chloroform solution (0.38 mM). More large-area TEM images are presented in Figures S7 and S8.

was also investigated for the self-assembly processed on the surface of glass through solvent-vapor annealing. Such a surface-assisted process was successfully used to fabricate high-quality nanobelts from a PTCDI molecule with a short, linear side chain (e.g., propoxyethyl).[57] The fabrication started with a thin film spin-cast on glass, followed by annealing the film in a closed chamber saturated with vapor of an appropriate solvent (e.g., chloroform). The size of the nanobelt thus fabricated depends mainly on the thickness of the film, which in turn is determined by the spinning speed and the concentration of the solution used for casting. Another factor critical to the fabrication processing is the roughness of the substrate surface. In this study, the glass surface cleaned by piranha reagent (30:70 H_2O_2(35%)/H_2SO_4) showed a roughness of only about 0.8 nm (Figure S10), which is much smaller than the dimensional size of the molecules and the molecular assembly. Such a flat surface is highly suitable for both the surface fabrication and microscopy measurement of the nanobelts, which have thickness in the range of 10 to a few tens of nanometers.

Figure 11A shows an AFM image of the nanobelts of DD-PTCDI fabricated from annealing of a thin film in chloroform vapor for 12 h. The thickness of the nanobelts thus fabricated is only about 8 nm (Figure S11), much smaller than that fabricated in solutions. In general, it is challenging to fabricate such thin nanobelts in the solution phase. However, as previously observed for other PTCDI molecules,[57] the thickness of surface-supported self-assembly can feasibly be controlled by adjusting the thickness of the starting film, which in turn can be controlled by the speed of the spin-casting and/or the concentration of the solution. Scanning different areas over the sample revealed quite uniform width of the nanobelts. In contrast, under the same fabrication conditions, ND-PTCDI molecules formed only particles with size depending on the thickness of the starting film. Figure 11B shows a typical AFM image of the particulate aggregate of ND-PTCDI fabricated from a spin-cast film. Most of the particles are in the size range of 40−70 nm.

The self-assembly of molecules under solvent vapor annealing is principally due to the solvent-facilitated mobility of molecules,

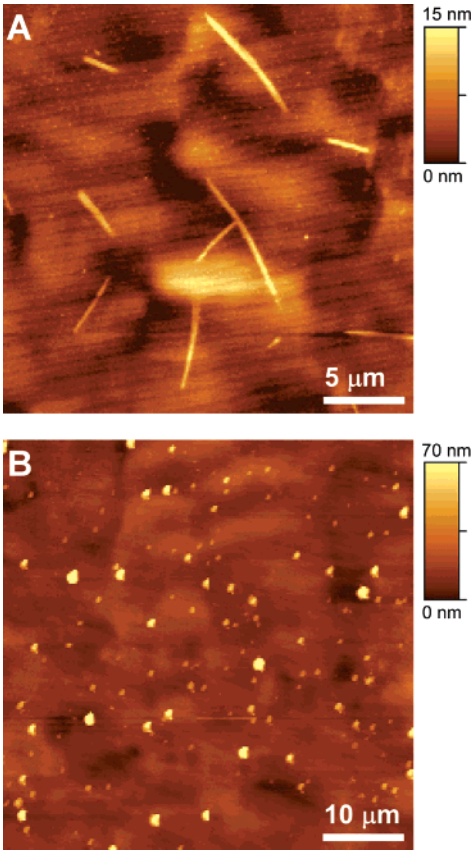

Figure 11. AFM image of DD-PTCDI nanobelts (A) and ND-PTCDI nanocrystals (B), both fabricated in situ on glass through chloroform vapor annealing. The starting thin film was prepared by spin-coating four drops of a chloroform solution (0.28 mM for DD-PTCDI, 0.5 mM for ND-PTCDI) onto a glass cover slip at a speed of 1500 rpm.

which enables molecules to reorganize into an energy-minimized conformation (the most stable state, which is determined by the molecular structure, particularly the side-chain structure) from the originally thermodynamically unstable state formed during the spin-casting (which provides fast evaporation). To this end, the distinct morphologies obtained for the assembly of the two molecules reveal the totally different molecular packing conformations, which are primarily determined by the molecular thermodynamics. Considering the same molecular backbone of the two molecules, the different molecular packing is most likely due to the side-chain interaction.

Conclusion

We have successfully investigated the side-chain effect on the molecular stacking conformation for two PTCDI molecules with distinct side-chain structures, linear vs branched alkyl chain. The linear chain provides minimized steric hindrance and the interchain hydrophobic interaction is cooperative with the $\pi-\pi$ stacking between the PTCDI backbones. In contrast, the swallow-tail-like chain brings significant steric hindrance, and distorts the molecular stacking from the co-facial configuration, presenting the molecules from assembling along one dimension. The side-chain effect on the molecular assembly has been characterized by comparative measurements of the optical spectra, differential calorimetry, fluorescence microscopy, and X-ray diffraction. The different molecular interactions (stacks) produce different morphologies of the molecular aggregate, 1D nanobelt for DD-PTCID and 0D nanosphere for ND-PTCDI. The strong $\pi-\pi$ stacking makes the fabricated nanobelts robust for being transferred to a solid substrate without perturbation of the morphology.

1D molecular aggregation demands a concerted interplay between the thermodynamics and processing kinetics of molecules. The global morphology of molecular aggregate of PTCDI is determined by the energy-minimized conformation of molecular stacking, which is favored by linear side-chain structure due to the decreased steric hindrance. However, to achieve such a thermodynamically optimal stacking conformation, it is essential to balance the processing parameters to provide the molecules with sufficient time to accommodate the optimal conformation in stacking. To this end, the presented investigation provides some alternatives for the future fabrication of dimensionally controlled nanostructures of PTCDI molecules.

1D organic semiconductor nanostructures provide enormous prospective applications in optoelectronic devices. The nanowires fabricated in this study are currently being employed in the application studies involving both electrical and optical properties. For example, the examination of the photocurrent of single nanowires (particularly in response to polarized light) will lead to potential applications in photodiode, sensor, and other orientation-sensitive optical devices. Moreover, the strong $\pi-\pi$ stacking and the long-range molecular organization would provide the nanowire with feasibly detectable conductivity, which in turn is expected to be dependent on the local electrical field due to the modulation on the π-electron delocalization. Such properties will enable us to fabricate new types of field-effect transistors based on n-type organic channels.

Acknowledgment. This paper is dedicated to Professor Michael A. J. Rodgers on the occasion of his 70th birthday. The work was supported by Consortium for Advanced Radiation Sources (CARS), and ORDA, COS, and MTC of SIUC. X-ray diffraction was carried out in the Center for Microanalysis of Materials (CMM), University of Illinois, which is partially supported by the U.S. Department of Energy under Grant No. DEFG02-91-ER45439. J.Z. and L.Z. thank NSFC (No. 20520120221) and K. C. Wong Foundation for support. We thank Prof. Dan Dyer for generous access to his DSC, and Irene Kiragu and Prof. Matt McCarroll for the assistance in solid-state fluorescence measurement in their lab. We also thank Mr. Steven Schmitt and Prof. John Bozzola at SIU IMAGE center for the help in SEM and TEM imaging and Dr. Mauro Sardela at CMM for the assistance in X-ray measurement.

Supporting Information Available: Experimental details; UV−vis absorption and fluorescence spectra of the ND- and DD-PTCDI in various solvents and under different temperatures (Figures S1−3); more SEM images of self-assemblies (Figures S4−5); fluorescence microscopy image of nanobelts of DD-PTCDI under shorter wavelength excitation (Figure S6); more TEM images of nanobelts of DD-PTCDI deposited on silicon oxide (Figure S7) and holey carbon (Figure S8) films; one more AFM image of DD-PTCDI deposited on glass (Figure S9); an AFM image of the glass surface cleaned by piranha reagent (Figure S10); and line-scan profiles of the AFM image shown in Figure 13A (Figure S11). This material is available free of charge via the Internet at http://pubs.acs.org.

JA061810Z